Matching Synchronous Machine Control for Improving Active Support of Grid-forming PV Systems with Enhanced DC Voltage Dynamics

Zizhen Guo, *Student Member*, *IEEE*, and Wenchuan Wu, *Fellow*, *IEEE*

***Abstract*—With photovoltaic (PV) sources becoming more prevalent in the energy generation mix, transitioning grid-connected PV systems from grid-following (GFL) mode to grid-forming (GFM) mode becomes essential for offering self-synchronization and active support services. Although numerous GFM methods have been proposed, the potential of DC voltage control malfunction during the provision of the primary and inertia support in a GFM PV system remains insufficiently researched. To fill the gap, some main GFM methods have been integrated into PV systems featuring detailed DC source dynamics. We conduct a comparative analysis of their performance in active support and DC voltage regulation. AC GFM methods such as virtual synchronous machine (VSM) face a significant risk of DC voltage failure in situations like alterations in solar radiation, leading to PV system tripping and jeopardizing local system operation. In the case of DC GFM methods such as matching control (MC), the active support falls short due to the absence of an accurate and dispatchable droop response. To address the issue, a matching synchronous machine (MSM) control method is developed to provide dispatchable active support and enhance the DC voltage dynamics by integrating the MC and VSM control loops. The active support capability of the PV systems with the proposed method is quantified analytically and verified by numerical simulations and field tests.**

***Index Terms*—Active support, DC voltage dynamics, grid-forming (GFM), matching control, photovoltaic (PV), virtual synchronous machine.**

I. INTRODUCTION

OVER the past decade, the penetration level of photovoltaic (PV) sources in the distribution network has increased as a result of lower equipment costs and clean energy policies [1]. Consequently, the distribution network is undergoing a significant transition from the passive systems to low inertial active systems based on nearly 100% renewable energy [2], which poses serious near-term challenges to the frequency and voltage stability of power systems [3].

Currently, most PV sources operate in the maximum power point tracking (MPPT) mode to harvest the maximum solar power, and the interfacing converters are controlled in grid-following (GFL) mode to deliver the exact solar power. As a result, the PV sources not only lack a dynamic response to system disturbance but are also prone to large-scale tripping due to a number of failures, which further exacerbates the instability risk to the utility grid [4]. To deal with this issue, grid codes in countries such as China, Germany, and Romania have specified the requirements for the frequency and voltage regulation of the grid-connected large-scale PV power plants [5].

Several control strategies have been proposed for GFL PV sources to provide active power support. Through power reserve control [6] or energy storage incorporation [7], the active power from PV sources can response to the local frequency deviation to provide the power droop support [8] and response to the rate of change of frequency (RoCoF) to generate the virtual inertia (VI) [9]. However, the process of local frequency measurement introduces an inevitable delay to the control loop of active power support, leading to the degraded performance of the emulated VI [10]. Though it is possible to modify GFL converters to provide ancillary services, synchronization units such as phase-locked loop (PLL) units may introduce undesired instability under weak grid conditions [11], hindering their applications in low-voltage networks.

To deal with this issue, the grid-forming (GFM) control has attracted increasing interest. While the definition of GFM converters has not been officially defined, its features can approximate a voltage source such as a synchronous generator (SG) [12], which makes the grid-support services include inertia [13], damping [14], primary support [15], voltage regulation [16], and black start [17]. A key difference between GFL and GFM modes is that the former needs the voltage phasor from the utility grid to synchronize the current injection, while the latter operates independently as a voltage source, enabling the island-mode operation of GFM sources [18].

Among the existing GFM methods, the droop control is a classic method in stand-alone microgrids for load sharing between GFM converters, which mimics the governor droop characteristic of SGs [19]. To further emulate the inertia response, the virtual synchronous machine (VSM) method is

Manuscript received: September 2, 2023; revised: December 19, 2023; accepted: May 8, 2024. Date of CrossCheck: May 8, 2024. Date of online publication: June 21, 2024.

This work was supported in part by the National Key R&D Program of China (No. 2022YFB2402900) and the National Natural Science Foundation of China (No. U2066601).

Z. Guo and W. Wu (corresponding author) are with the State Key Laboratory of Power Systems, Department of Electrical Engineering, Tsinghua University, Beijing 100084, China (e-mail: gzz1998@126.com; wuwench@tsinghua.edu.cn).

DOI: 10.35833/MPCE.2023.000624

proposed to emulate the swing equation of SG to provide short-term VI [20]. In contrast to the droop control and VSM methods, which emulate SG dynamics from the AC side of the converter, [21] proposes a matching control (MC) method by adapting DC voltage dynamics with swing dynamics. The structural similarity also shows the physical realization behind the VI, which is derived from the DC bus capacitance. Similarly, [13] utilizes the DC voltage dynamics to provide the inertia and droop response while regulating the DC voltage. But the differential term of DC voltage may cause the numerical instability in real-time control. To synchronize parallel converters, [22] proposes the virtual oscillator control (VOC) method, where each converter behaves as a nonlinear oscillator to maintain global asymptotic synchronization. Since the power injection under VOC cannot be specified, dispatchable virtual oscillator control (dVOC) is proposed to realize the secondary power regulation based on local set-points [23], [24].

The aforementioned GFM methods can be classified into two categories: AC GFM and DC GFM. For AC GFM methods like droop control, VSM, and dVOC, the AC measurements such as the output current and power are fed back to regulate the synchronous speed to provide active support. It is assumed that the DC voltage dynamics are well regulated, which may be true for battery energy storage systems (BESSs), but not for PV systems [25]. In AC GFM PV systems, the aggressive active support may lead to DC voltage collapse and modulation failure. For DC GFM methods like MC, the DC voltage dynamics are utilized for the synchronization, and thus the steady-state error of DC voltage is inevitable after the primary response. Due to the strong coupling between DC dynamics on the primary side and AC performance on the inverter side, it is challenging to precisely track the specified target for the active support indices such as inertia constants and droop ratios in DC GFM methods. While for AC GFM methods, the active support is naturally dispatchable through the AC measurement feedback.

It is evident that the integration of AC and DC GFM methods represents a fruitful avenue for the exploitation of the respective advantages inherent to the two distinct categories of GFM methods. In [26], an adaptive dynamic droop scheme is proposed for a single-stage PV system, in which the DC voltage is regulated in the power angle loop. Similarly, in [27], a voltage-based droop control is developed for power sharing in resistive microgrid. In [28], a multi-input-multi-output GFM method based on the unified multivariable transfer matrix is proposed, revealing that the coupling of DC voltage dynamics and power angle loop facilitates the damping of DC voltage oscillations. The AC/DC dual-port interactions are also exploited in high-voltage direct current (HVDC) applications in [29]. However, the impact of DC voltage regulation on the active support performance is not considered in these studies. Once the interaction mechanism between DC dynamics and AC transients is illustrated, it should be possible to achieve improved active support performance of GFM PV systems with enhanced DC voltage dynamics [30].

The adaptation of GFM methods to PV systems is constrained by two main considerations: the limited energy capacity and power capacity. The issue of energy capacity pertains to the limited DC-link energy storage and the intermittent nature of solar energy. This necessitates the use of deloaded PV system [15], [31] or additional energy storage systems in parallel [25], [32] to provide flexibility in the primary source. The issue of power capacity pertains to the prominent overcurrent observed during large disturbances under limited power delivery capacity of inverters. A current limitation scheme embedded in the low-level cascaded voltage-current control loop [33] has been the subject of extensive study, with the objective of protecting the power switches from the damage caused by overcurrent.

In this paper, we compare and evaluate the main GFM methods on their active support performance based on a two-stage deloaded PV system. The risk of DC voltage collapse of AC GFM methods is revealed, and the corresponding enhancements are made through the joint feedback of DC and AC signals. The contributions of this work are threefold:

1) The interactions between the DC voltage dynamics driven by the nonlinear primary source and the AC active support transients driven by frequency events in two-stage GFM PV systems are revealed by detailed simulations and discussions, which tend to be oversimplified in previous studies.

2) A matching synchronous machine (MSM) control method is developed to improve the active support of GFM PV systems with enhanced DC voltage dynamics, which combines the merits of the MC and VSM.

3) The impact of DC voltage regulation on the active support from GFM PV systems is explicitly quantified in the proposed method while previous studies often treat DC and AC performance separately.

The remainder of this paper is organized as follows. In Section II, the dynamic model of PV systems is presented. Section III reviews the main GFM methods of interest and presents the proposed MSM control method. In Section IV, the active support characteristics of various GFM methods and their interactions with PV dynamics are discussed in the case studies. Section V draws the conclusion.

II. Dynamic Model of PV Systems

The two-stage PV system is considered in this study, which differs from the single-stage PV system with an additional boost converter to regulate the PV voltage. As shown in Fig. 1, the PV array outputs photocurrent, the boost converter is controlled to regulate the DC voltage, and the inverter is controlled using GFM methods to be integrated. E_r and T are the solar irradiance and temperature, respectively; v_{pv} is the PV voltage; i_{pv} is the output current; v_{dc} is the DC-link voltage; i_{dc} is the DC input current; D is the conduction ratio; C_{dc} is the DC-link capacitance; L_g and R_g are the line parameters through which the PV system is integrated to the utility grid; δ is the phase angle shift; $\boldsymbol{i}_{o,dq}=\left[i_{od}, i_{oq}\right]^{\mathrm{T}}$ is the output current of the inverter in dq-coordinate; $\boldsymbol{v}_{i,dq}=\left[v_{id}, v_{iq}\right]^{\mathrm{T}}$ is the node voltage of the inverter in dq-coordinate; v_m and θ are the magnitude and the phase angle of the inverter voltage, respectively; and V_g is the voltage magnitude of the power gird.

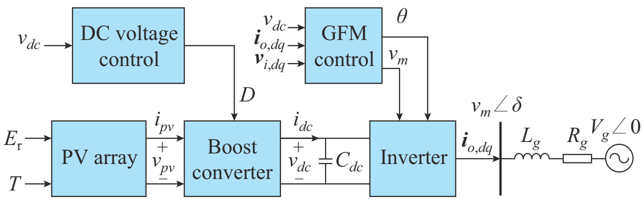

Fig. 1. Schematic diagram of a two-stage GFM PV system.

A. PV Array

The PV array is composed of multiple PV modules, which are connected in series and parallel. The PV array is modeled through the practical engineering model [34]. Given the values of open-circuit voltage V_{oc}, short-circuit current I_{sc}, and the maximum operation point (V_{mp}, I_{mp}), the output characteristic of the PV array is described as:

$$i_{pv}=f\left(v_{pv}\right)=I_{sc}\left(1-\exp\left(C_1\left(v_{pv}-V_{oc}\right)\right)\right) \tag{1}$$

$$C_1=\frac{1}{V_{mp}-V_{oc}}\ln\left(1-\frac{I_{mp}}{I_{sc}}\right) \tag{2}$$

where f denotes the nonlinear PV output characteristic. The parameters $\left(V_{oc}, I_{sc}, V_{mp}, I_{mp}\right)$ are provided under the standard test condition (STC) and the corresponding details are shown in Supplementary Material A.

B. Boost Converter

In GFL MPPT mode, the boost converter regulates the PV voltage to facilitate the maximum extraction of solar power. While in GFM PV system, the boost converter is responsible for DC voltage control. In order to enhance the calculation efficiency in power system studies, the switching transients inside converters are neglected. In typical frequency events, the time constant of boost converter transients is significantly smaller than that of the DC voltage dynamics [35]. Therefore, the steady-state equation is used:

$$v_{pv}=\left(1-D\right)v_{dc} \tag{3}$$

$$i_{dc}=\left(1-D\right)i_{pv} \tag{4}$$

We use a proportional-integral (PI) controller in the boost converter for the DC voltage control. The model of the controller is given by:

$$D=k_p\left(v_{dcN}-v_{dc}\right)+k_i\int_0^t\left(v_{dcN}-v_{dc}\right)\mathrm{d}\tau \tag{5}$$

where k_p and k_i are the proportional and integral control gains, respectively; and v_{dcN} is the nominal DC voltage.

C. DC-link Capacitor

The dynamic model of the DC-link capacitor is given as:

$$C_{dc}\frac{\mathrm{d}v_{dc}}{\mathrm{d}t}=i_{dc}-\frac{p_{ac}}{v_{dc}} \tag{6}$$

$$p_{ac}=v_{id}i_{od}+v_{iq}i_{oq} \tag{7}$$

where p_{ac} is the output active power of the inverter. Note that the inverter efficiency is considered sufficiently high to allow for the power loss through it to be neglected.

D. Inverter

The switching transients of the inverter are neglected, as they typically occur at frequencies above 10 kHz. The fundamental frequency model of the inverter current is presented in dq-coordinate as:

$$L_g\frac{\mathrm{d}i_{od}}{\mathrm{d}t}=v_{id}-V_{gd}-R_gi_{od}+\omega_nL_gi_{oq} \tag{8}$$

$$L_g\frac{\mathrm{d}i_{oq}}{\mathrm{d}t}=v_{iq}-V_{gq}-R_gi_{oq}-\omega_nL_gi_{od} \tag{9}$$

where V_{gd} and V_{gq} are the voltages of point of common coupling (PCC) in dq-coordinate; and ω_n is the nominal frequency.

It is worth noting that the filter dynamics are assumed to be well damped by the feedforward design in low-level cascaded voltage-current control. Given that the focus is on the timescale of DC link, it is assumed that the inner voltage-current control will track the voltage reference from GFM methods ideally [36].

III. Main GFM Methods and Proposed MSM Control Method

In this section, three GFM methods, including VSM, MC, and dVOC, are reviewed, and the proposed MSM control method is presented. Since the focus of this paper is to evaluate the active support capability of the GFM PV system, the voltage loop of previous GFM methods is simplified. Readers with interests in these voltage loop designs can refer to [30] for more details.

A. VSM

There are several variations of VSM methods to emulate different numerical models of SG. For details on these variations, please refer to [37]. In this paper, we focus on the basic VSM model, which mimics the swing equation of SG as shown in Fig. 2, where T_a is the time constant of the VI; ω is the synchronous speed; p^{ref} is the active power reference; $\Delta\omega_{ac}$ is the frequency adjustment by the AC-side active power; and D_p is the droop gain rather than the damping coefficient because the nominal frequency ω_n is a constant setpoint rather than the actual grid frequency.

$$T_a\omega_n\frac{\mathrm{d}\omega}{\mathrm{d}t}=p^{ref}-p_{ac}-D_p\left(\omega-\omega_n\right) \tag{10}$$

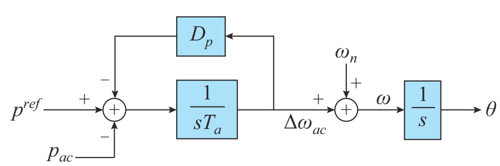

Fig. 2. Control diagram of VSM.

B. MC

MC is implemented by matching the DC voltage dynamics with the SG dynamics. Assuming that DC voltage is close to its reference value, (6) is reformulated as:

$$C_{dc}v_{dcN}\frac{\mathrm{d}v_{dc}}{\mathrm{d}t}=p_{dc}-p_{ac} \tag{11}$$

where p_{dc} is the power input from the primary source. Inspect (10) and (11), if the frequency is driven by the DC voltage through a constant k_m, as shown in (12), then the power-frequency dynamics of MC are given as (13).

$$\begin{cases} \omega = k_m v_{dc} \\ k_m = \dfrac{\omega_n}{v_{dcN}} \end{cases} \tag{12}$$

$$\frac{C_{dc}}{k_\theta^2}\omega_n \frac{\mathrm{d}\omega}{\mathrm{d}t} = p_{dc} - p_{ac} \tag{13}$$

Comparing (10) and (13), the structural matching between the DC voltage dynamics and the SG dynamics is revealed. The DC-link capacitance serves as the internal energy storage to provide the equivalent inertia with a time constant of C_{dc}/k_m^2. It is worth noting that the VI of MC is constrained by the small DC-link capacitance. The matching ratio k_θ can be relaxed to enhance the equivalent inertia [38].

However, the equivalent droop response in (13) differs from that of the ideal MC due to the strong nonlinearity of PV array. With a first-order Taylor expansion of input power p_{dc} around the normal frequency ω_n, we can obtain:

$$\frac{C_{dc}}{k_m^2}\omega_n \frac{\mathrm{d}\omega}{\mathrm{d}t} = p_{dc}\left(\omega_n\right) - p_{ac} + \frac{\partial p_{dc}\left(\omega_n\right)}{\partial \omega}\left(\omega - \omega_n\right) \tag{14}$$

$$\frac{\partial p_{dc}\left(\omega_n\right)}{\partial \omega} = \frac{I_{sc}}{k_m^2}\left(k_m + k_p\omega_n\right)\left[1 - \left(1 + C_1 v_{dc}^{ref}\right)\mathrm{e}^{C_1\left(v_{dc}^{ref} - V_{oc}\right)}\right] \tag{15}$$

where v_{dc}^{ref} is the DC voltage reference.

It can be observed that the equivalent small-signal droop gain varies with both the DC voltage control parameters and the weather-dependent PV parameters, which makes the droop response of the GFM PV system intractable in the MC mode. Meanwhile, the strong nonlinearity of the output characteristic of the PV array leads to the undesired nonlinear droop behavior of GFM PV systems under large disturbances. It is worth mentioning that the integral coefficient k_i of boost control in MC mode should be set to be zero to prevent unstable power regulation, since the steady-state error of DC voltage always exists after the primary droop response.

C. dVOC

dVOC [23], [39] is capable of achieving almost global asymptotic stability, which implies that global synchronization can be attained under a wide range of initial phase shift conditions. The dynamics of dVOC in $\alpha\beta$-coordinate are given by [24]:

$$\frac{\mathrm{d}\boldsymbol{v}_{i,\alpha\beta}}{\mathrm{d}t} = \omega_n \boldsymbol{\mathcal{J}} \boldsymbol{v}_{i,\alpha\beta} + \eta\left(\boldsymbol{\mathcal{K}}\boldsymbol{v}_{i,\alpha\beta} - \boldsymbol{\mathcal{R}}(\kappa)\boldsymbol{i}_{o,\alpha\beta}\right) + \phi\left(v_m\right)\boldsymbol{v}_{i,\alpha\beta} \tag{16}$$

$$\boldsymbol{\mathcal{R}}(\kappa) = \begin{bmatrix} \cos(\kappa) & -\sin(\kappa) \\ \sin(\kappa) & \cos(\kappa) \end{bmatrix} \tag{17}$$

$$\begin{cases} \boldsymbol{\mathcal{J}} = \boldsymbol{\mathcal{R}}(\pi/2) \\ \boldsymbol{\mathcal{K}} = \dfrac{1}{V_n^2}\boldsymbol{\mathcal{R}}(\kappa)\begin{bmatrix} p^{ref} & q^{ref} \\ -q^{ref} & p^{ref} \end{bmatrix} \end{cases} \tag{18}$$

$$\phi\left(v_m\right) = \mu \frac{V_n^2 - v_m^2}{V_n^2} \tag{19}$$

where $\boldsymbol{v}_{i,\alpha\beta} = \left[v_{i\alpha}, v_{i\beta}\right]^{\mathrm{T}}$ is the inverter voltage reference; V_n is the nominal voltage magnitude; $\boldsymbol{i}_{o,\alpha\beta} = \left[i_{o\alpha}, i_{o\beta}\right]^{\mathrm{T}}$ is the inverter output current; η, μ, and κ are the design parameters; and q^{ref} is the reactive power set-point. Formula (16) can be interpreted in three components: $\omega_n \boldsymbol{v}_{i,\alpha\beta}$ represents the synchronous oscillator, $\boldsymbol{v}_{i,\alpha\beta} - \boldsymbol{\mathcal{R}}(\kappa)\boldsymbol{i}_{o.\alpha\beta}$ represents the phase error, and $\phi\left(v_m\right)$ represents the magnitude error.

As mentioned before, the voltage magnitude reference is set at the nominal value to eliminate the reactive power loop, i.e., $v_m = V_n$. Choosing $\kappa = \pi/2$ and rewriting (16) in polar coordinates, the ω-P droop characteristic of dVOC is given as:

$$\omega = \omega_n + \frac{\eta}{V_n^2}\left(p^{ref} - p_{ac}\right) \tag{20}$$

where V_n^2/η is the equivalent droop ratio.

D. MSM

From the standpoint of active support, GFM methods of droop control, VSM, and dVOC focus on the AC-side interfacing characteristics. However, in reality, the active support behavior demanded by GFM methods necessitates the physical support provided by the inverter. When the power demanded by the GFM method exceeds the available primary power, the internal DC voltage stability is threatened. MC has the ability to regulate the DC voltage because the power angle of MC is adjusted to compensate for the power imbalance on the DC link. However, the droop support of MC in (12) is not dispatchable and its inertia is constrained by the DC-link capacitance. In order to address this issue, the MSM based on the joint feedback of AC power and DC voltage is proposed:

$$T_a \omega_n \frac{\mathrm{d}\omega}{\mathrm{d}t} = p^{ref} - p_{ac} - D_p\left(\omega - \omega_n - k_\theta \Delta v_{dc}\right) \tag{21}$$

$$\Delta v_{dc} = v_{dc} - v_{dc}^{ref} \tag{22}$$

where k_θ is the variable matching factor to adjust the inertia from DC-link capacitance; and Δv_{dc} is the DC voltage deviation. The AC voltage magnitude is controlled by a PI controller to provide reactive support.

As shown in Fig. 3, the frequency signal is driven by the dispatchable active support and the DC voltage regulation simultaneously. In Fig. 3, V_{ac}^{ref} is the reference of the AC-side voltage magnitude; k_{pv} and k_{iv} are the proportional and integral control parameters of voltage loop, respectively; and $\Delta\omega_{dc}$ is the frequency adjustment by the DC-link voltage. With the feedback from AC-side active power, the desired active support characteristic is emulated. When considerable DC-link power imbalance occurs, the deviated DC voltage signal is transmitted to the inverter frequency adjustment to regulate the power angle and to compensate for the power imbalance. With merging AC and DC feedbacks in GFM designs, MSM can provide the dispatchable active support while stabilizing the DC voltage dynamics.

In steady state, the DC voltage is regulated to its reference value by the PI controller of the boost converter. Therefore, the ω-P droop characteristic of MSM is given as (23), which indicates the dispatchable droop characteristic of MSM.

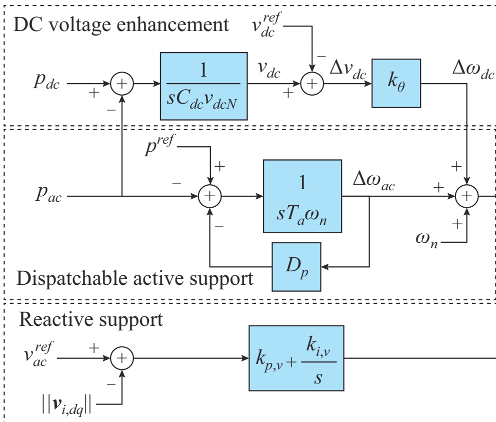

Fig. 3. Control diagram of MSM.

$$\omega=\omega_n+\frac{1}{D_p}\left(p^{ref}-p_{ac}\right) \tag{23}$$

Then, we analyze the inertia provided by the MSM considering the impact of DC voltage dynamics. By ignoring the droop response, we can derive the transfer functions from AC and DC feedbacks separately:

$$H_{ac}(s)=\frac{\Delta\omega_{ac}(s)}{p_{ac}(s)}=\frac{1}{sT_a\omega_n} \tag{24}$$

$$H_{dc}(s)=\frac{\Delta\omega_{dc}(s)}{p_{ac}(s)}=\frac{k_\theta}{sC_{dc}v_{dcN}} \tag{25}$$

Define the equivalent inertia from matching loop as:

$$T_m=\frac{C_{dc}v_{dcN}}{k_\theta\omega_n} \tag{26}$$

The sum of (24) and (25) yields (27), which indicates that the equivalent inertia of MSM is affected by the DC voltage regulation in a harmonic mean manner.

$$H(s)=\frac{\Delta\omega(s)}{p_{ac}(s)}=\frac{1}{sT_a\omega_n}+\frac{1}{sT_m\omega_n}=\frac{T_a+T_m}{sT_aT_m\omega_n} \tag{27}$$

Since the inertia from DC link is usually smaller due to limited DC-link capacitance, the additional loop of DC voltage enhancement decreases the overall inertia provided by GFM PV systems. Table I presents a comparison between MSM and GFM methods. Compared with DC GFM methods, MSM offers the dispatchable active support in both inertia support and droop response, as shown in (23) and (27). While compared with AC GFM methods, the DC voltage dynamics are enhanced by the DC voltage feedforward signal in the power angle loop.

TABLE I
COMPARISON BETWEEN MSM AND GFM METHODS

Method	Dispatchable active support capability		DC voltage enhancement
	Inertia support	Droop response	
Droop	×	√	×
VSM	√	√	×
MC	×	×	√
dVOC	×	√	×
MSM	√	√	√

To evaluate the stability of the proposed method, the small-signal dynamic model of the GFM PV system is derived. The derivation details are included in Supplementary Material B.

$$\frac{\mathrm{d}\boldsymbol{x}}{\mathrm{d}t}=\begin{bmatrix} 0 & 1 & 0 & 0 & 0 & 0 \\ 0 & -\frac{D_p}{T_a\omega_n} & -\frac{v_{id}^*}{T_a\omega_n} & 0 & \frac{k_\theta D_p}{T_a\omega_n} & 0 \\ \frac{V_g}{L_g}\sin\delta^* & 0 & -\frac{R_g}{L_g} & \omega_n & 0 & 0 \\ \frac{V_g}{L_g}\cos\delta^* & 0 & -\omega_n & -\frac{R_g}{L_g} & 0 & 0 \\ 0 & 0 & -\frac{v_{id}^*}{C_{dc}v_{dc}^*} & 0 & \lambda_1 & \lambda_2 \\ 0 & 0 & 0 & 0 & -1 & 0 \end{bmatrix}\boldsymbol{x}$$

$$\boldsymbol{x}=\begin{bmatrix}\hat{\delta} & \hat{\omega} & \hat{i}_{od} & \hat{i}_{oq} & \hat{v}_{dc} & \hat{\phi}\end{bmatrix} \tag{28}$$

$$\lambda_1=\frac{u_{id}^*i_{od}^*}{C_{dc}\left(v_{dc}^*\right)^2}+\frac{k_p i_{pv}^*}{C_{dc}}+\frac{v\left(1-D^*\right)\left(1-D^*+k_p v_{dc}^*\right)}{C_{dc}} \tag{29}$$

$$\lambda_2=-\frac{k_i i_{pv}^*}{C_{dc}}-\frac{vk_i v_{dc}^*\left(1-D^*\right)}{C_{dc}} \tag{30}$$

$$v=\frac{C_1\ln\left(i_{pv}^*-I_{sc}\right)}{V_{mp}-V_{oc}} \tag{31}$$

where ϕ is the integral variable of boost converter controller; and the symbols $\wedge$ and * represent the incremental value and steady-state value of corresponding variables, respectively.

From the small-signal model, it can be seen that, the only difference between MSM and VSM is the off-diagonal term $k_\theta D_p/\left(T_a\omega_n\right)$ that links the DC voltage dynamics with the power-frequency loop. When the fast-vanishing dynamics are not considered, the closed-loop pole trajectories of the GFM PV system controlled with the MSM are shown in Fig. 4. When the matching factor increases, both the synchronous oscillation (SO) mode and VI mode move toward the stable region. This indicates that the additional DC voltage feedforward on the power-frequency loop provides improved stability, particularly in the VI mode, since this mode most dominates the power exchange through DC-link capacitor during the active support procedure. Figure 4(b) provides an insight into the manner in which primary dynamics influence active support stability in GFM PV systems. When the initial PV operation point is elevated to achieve a deeper power reserve level, the equivalent control gain on the DC voltage is amplified due to the nonlinearity of PV power curves. Subsequent case studies in Section IV-B further validate this theoretical result.

IV. CASE STUDY

In this section, the active support performance of main GFM methods implemented on PV systems is evaluated. The test system shown in Fig. 5, which is modified from the medium-voltage microgrid network benchmark developed by CIGRE [40], is used in the following case studies.

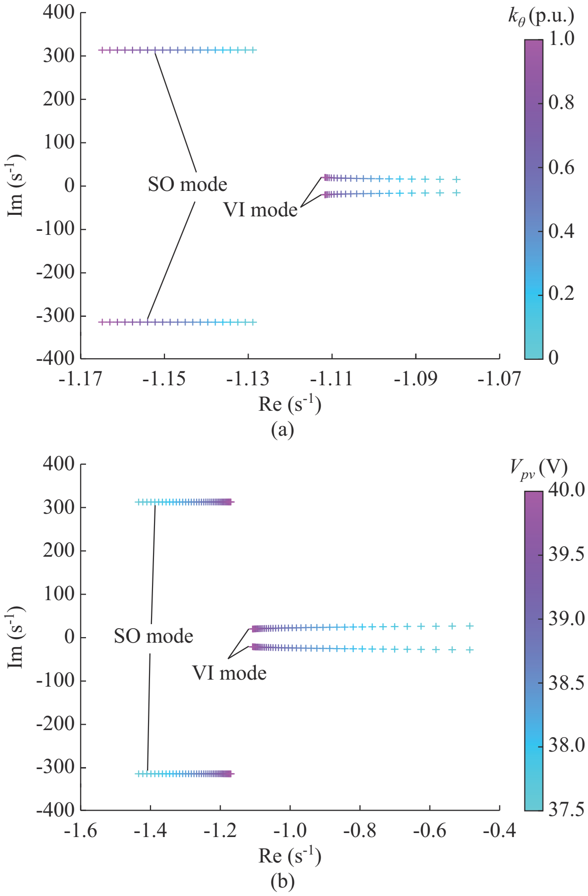

Fig. 4. Closed-loop pole trajectories of GFM PV system controlled with MSM. (a) Different matching factors. (b) Different PV deloading voltage levels.

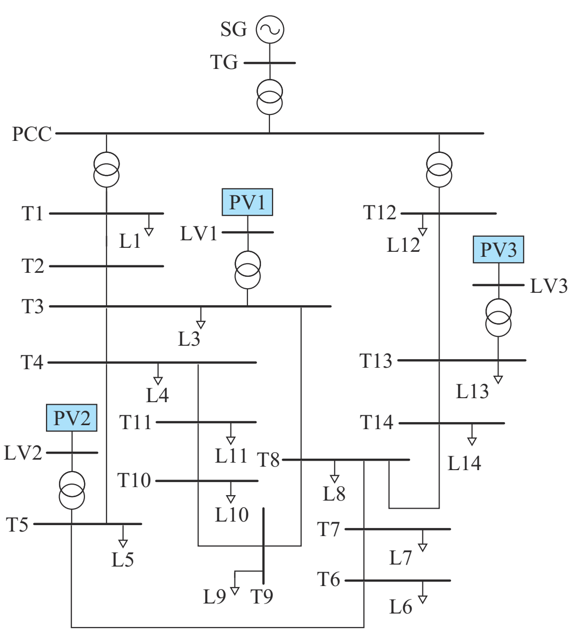

Fig. 5. Distribution network with GFM PV systems integrated.

The simulation is carried out on the DIgSILENT/PowerFactory software. The 8 MW SG is modeled using the fifth-order model, augmented with the IEEE T1 excitation system and the IEEE GT1 gas turbine governor. Three 2 MW distributed PV systems (PV1-PV3) are integrated at buses T3, T5, and T13. The total rated power of PV sources is 6 MW, which is 76% of the local load. The GFM mode in a PV system can be switched among VSM, MC, dVOC, and MSM. The initial active power of each PV source is set to be 80% of the maximum power to reserve a 20% power headroom for the active support. Some PV deloading control methods have been proposed in the literature [15], [31]. A simple method for PV deloading control is the pilot PV system, which is a PV system in GFL MPPT mode that searches for the maximum solar power for PV system groups. This method is also viable in practical applications. For the sake of simplicity, we omit the details of the power reserve control and assume that the accurate deloading operation of PV systems occurs under the initial condition. The deloading setting is defined as:

$$P_{ini} = rP_{mp} \tag{32}$$

where r is the deloading ratio; and P_{ini} and P_{mp} are the initial power set-point and the maximum power of PV system, respectively.

A. VI and Primary Droop Characteristics

We inspect the active support from GFM PV systems, including VI and primary droop responses. The equivalent droop ratio of dVOC is tuned to be identical to that of MSM and VSM, i.e., $\eta = V_n^2/D_p$, to exhibit identical droop behavior. As discussed in Section III-D, the droop response of MC is nonlinear and intractable, so the effective droop ratio of MC cannot be specified. To trigger the active support, a 10% load step disturbance is assigned at $t=1.0$ s to all load buses. The frequency at the PCC is recorded to represent the system frequency dynamics. The calculation of RoCoF is defined as:

$$\frac{\Delta\omega}{\Delta t} = \frac{\omega(t+\Delta t) - \omega(t)}{\Delta t} \tag{33}$$

where $\Delta\omega$ is the change of frequency; and $\Delta t = 250$ ms is the calculation window of RoCoF [30].

As shown in Fig. 6 and Table II, GFM PV systems provide active support following a load step change to regulate the system frequency. In light of the frequency nadir, MSM outperforms other GFM methods in providing stronger primary support. In Fig. 6(b), VSM, dVOC, and MSM present similar steady-state power responses due to the same droop setting. MSM provides inertia support by the amount between VSM and MC, which conforms to the relationship in (27). MC provides the smallest inertia due to the limited DC-link capacitance, as shown in (13). It is worth noting that the RoCoF of dVOC is improved, which indicates that the droop characteristics alone can provide a certain amount of inertia. This is because the active power is regulated in a short time scale that is closely aligned with the SG inertia dynamics. Figure 6(c) illustrates that the DC voltage of MSM is improved compared with VSM due to the additional DC voltage regulation. The steady-state error of DC voltage exists in MC because of the matching relationship between the frequency and the DC voltage.

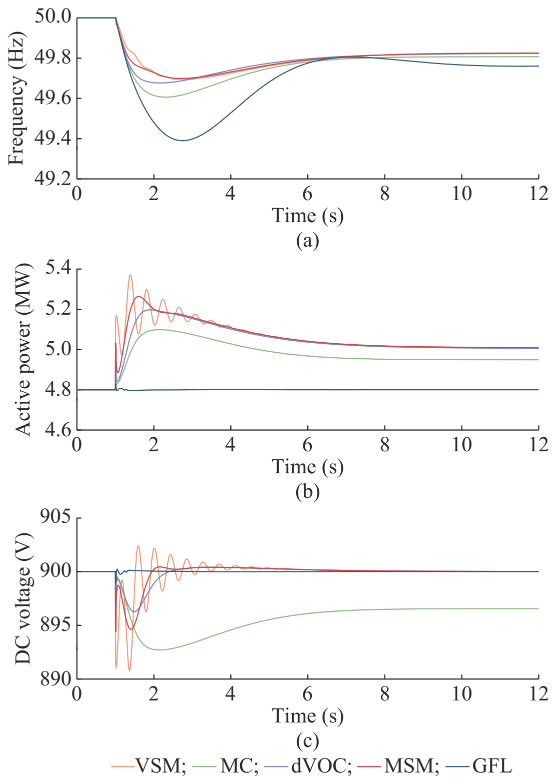

Fig. 6. Active support from PV systems under different GFM methods. (a) Frequency at PCC. (b) Total active power of PV systems. (c) DC-link voltage of single PV system.

TABLE II
COMPARISON OF ACTIVE SUPPORT PERFORMANCE OF DIFFERENT GFM METHODS

Method	Primary droop support		The maximum RoCoF (Hz/s)
	Frequency nadir (Hz)	Steady frequency (Hz)	
GFL	49.390	49.765	–0.802
VSM	49.695	49.826	–0.538
MC	49.606	49.808	–0.763
dVOC	49.677	49.825	–0.733
MSM	49.699	49.826	–0.660

B. DC Voltage Regulation

The design of GFM methods such as VSM and dVOC focuses on the AC-side interfacing characteristics. In practice, however, when the power demand of GFM methods exceeds the available primary power, the transient stability of the DC voltage is threatened. A variety of circumstances may result in a DC voltage collapse in GFM PV systems, including extreme weather conditions, inaccurate maximum power estimation, significant grid disturbances, and improper GFM parameter settings. Here, we inspect the active support performance of GFM PV systems in two scenarios to demonstrate the importance of DC voltage regulation.

1) Moving Cloud

Firstly, the changing weather is represented by a moving cloud that passes through distributed PV systems sequentially. Repetitive simulations with different GFM methods are conducted with a 10% load step disturbance at $t = 1.0$ s. As shown in Fig. 7(a), the moving clouds cause a rapid change in solar radiation, with a rate of change of 200 W/m^2 per second on each PV system, occurring sequentially from 1 to 6 s.

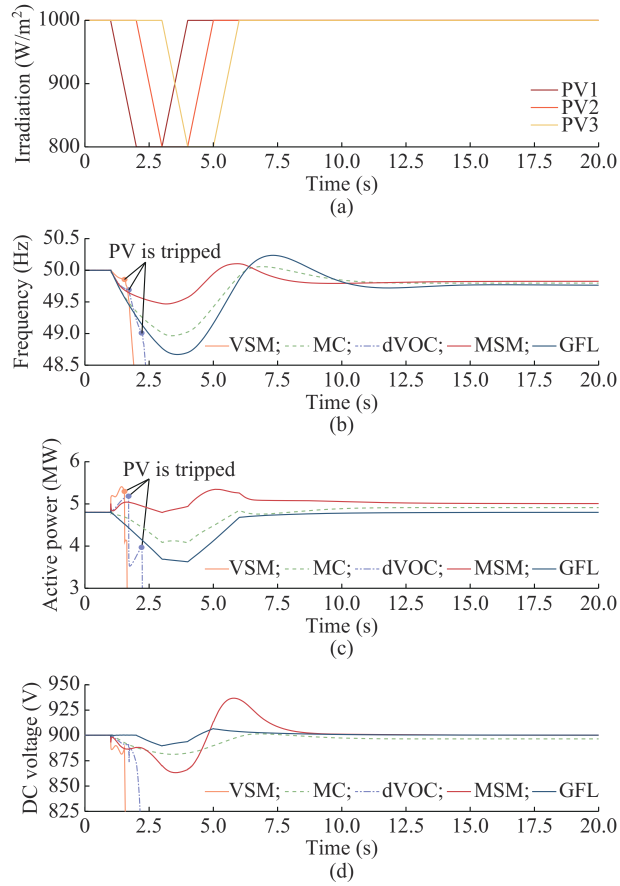

Fig. 7. Active support from PV systems with moving clouds. (a) Solar irradiation. (b) Frequency at PCC. (c) Total active power of PVs. (d) DC voltage of PV2.

This represents the highest rate of change observed in the context of moving clouds [41]. While the cloudy time overlaps with the GFM response process, the DC power of PV system is insufficient to provide the active support required by the VSM. Since VSM is agnostic to the DC voltage deviation, the power imbalance on the DC bus is further exacerbated by the aggressive inertia and primary control, resulting in the tripping of PV1 at $t = 1.6$ s, as shown in Fig. 7. Note that neighboring PV2 and PV3 are also tripped at almost the same time because their operation is coupled with PV1 by the system frequency, even though their local weather conditions have not yet changed. Similar tripping is also observed in the dVOC. Without the inertia response, the tripping of PV1 is delayed to 1.7 s, while PV2 and PV3 are tripped at 2.2 s. After PV system tripping, the frequency cannot be regulated by SG due to the high penetration of solar power, resulting in the microgrid blackout. Figure 7(c) and (d) indicates that, under MC and MSM, the DC voltage deviation affects the power angle, and the inverter power is dynamically adjusted to regulate the DC voltage. The difference is that MSM continues to provide active support, whereas the power curve of MC is analogous to the GFL mode, given that MC exhibits a robust correlation between its output performance and the DC voltage dynamics. It is worth mentioning that, after the weather transients, MSM can still accurately track the droop ratio and the steady-state frequency is consistent with that observed in Section IV-A, i.e., 49.826 Hz.

2) Load Step Disturbance

The percentage of load step is being gradually increased from 10% to 36% to test the active support performance of GFM PV systems under different levels of disturbances. As shown in Fig. 8, under VSM and dVOC, the maximum load step is 22% and 30%, respectively.

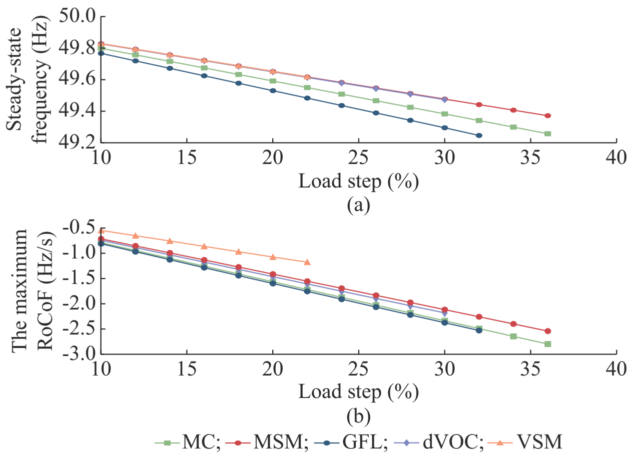

Fig. 8. Active support from PV systems with varying load step disturbances. (a) Steady-state frequency at PCC. (b) The maximum RoCoF at PCC.

When the load step increases, a comparable DC voltage collapse is observed, as illustrated in Fig. 7. The MC and MSM continue to provide the primary droop response to regulate the system frequency even under severe load changes of up to 36%. It is worth noting that, in the absence of active support, the system frequency does not attain a steady-state solution under GFL mode due to the load power flow exceeding the SG limit, which demonstrates the significance of active support from high-penetration PV sources. From Fig. 8(b), it can be observed that the inertia support from MSM effectively limits the RoCoF in contrast to MC. While VSM provides the greatest inertia under moderate disturbances, MSM manages to balance the transient response and the DC voltage dynamics to provide more reliable and stable active support.

C. Dispatchable Active Support of MSM

With the active power feedback of the inverter, the active support characteristic of MSM is dispatchable like other AC GFM methods such as droop control and VSM, which is more favorable in the coordination of large-scale distributed PV systems. As shown in Fig. 9, a series simulations are conducted to demonstrate the dispatchable active support from MSM, with the droop ratio varying from 10 to 50 p.u.. It can be observed that an increase in droop ratio results in enhanced primary support from GFM PV systems. Table III gives the statistical analysis of the active support performance, which demonstrates that the steady-state droop response of MSM precisely tracks the target frequency value. The target frequency is simulated by replacing distributed PV systems with ideal GFM inverters driven by an infinite DC bus. Figure 9(a) illustrates that the frequency nadir improvement under high droop ratio is less pronounced. Since the power angle of MSM is related to the DC voltage deviation, the droop response is dynamically adjusted to protect the DC voltage from over-support instability under severe disturbances.

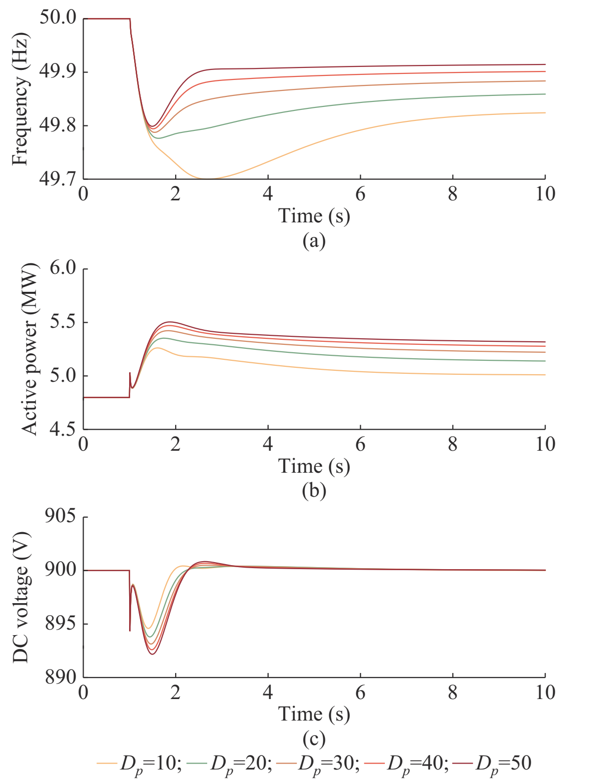

Fig. 9. Dispatchable active support from PV systems under MSM. (a) Frequency at PCC. (b) Total active power of PV systems. (c) DC voltage of single PV system.

TABLE III
DISPATCHABLE ACTIVE SUPPORT PERFORMANCE OF PV SYSTEMS UNDER MSM WITH VARIABLE DROOP RATIOS

Droop ratio (p.u.)	Primary droop support		The maximum RoCoF (Hz/s)
	Target frequency (Hz)	Steady-state frequency (Hz)	
10	49.826	49.826	–0.660
20	49.862	49.863	–0.653
30	49.886	49.887	–0.647
40	49.903	49.904	–0.642
50	49.916	49.916	–0.638

D. Effect of Primary Source Modeling

This subsection presents a demonstration of the impact of primary source modeling on the DC voltage dynamics of GFM PV systems. The prevailing modeling approach in the literature is to model the DC voltage as an ideal source. However, the physical constraints inherent to the real field are not considered in the ideal model. In [30], a controlled

DC current source (CS) is proposed to account for the power limitations. However, the nonlinearity of PV dynamics is not captured by the CS model, resulting in an incomplete description of the DC voltage dynamics.

To illustrate this nonlinearity, we apply VSM method to distributed PV systems and record the DC voltage dynamics during GFM transients under different power reserve levels r. Then, we reconduct the simulation with the primary source replaced from PV array to a CS. As shown in Fig. 10, the DC voltage dynamics driven by the CS model under different power reserve levels remain consistent, while for GFM PV systems, the change in deloading ratio makes a difference. This is because in the CS model, the PI parameters for DC voltage regulation are constant, whereas in the PV case, the equivalent regulation is variable due to the nonlinearity, as shown in Fig. 11, where P_{pv} is the output power of PV array; and P_{mp} is the maximum output power of PV array. Note that as the power reserve level decreases, the regulation of DC voltage by the primary source becomes stronger, which is consistent with the previous small-signal analysis. Once the operating point of PV array passes through the maximum power point, the primary source may destabilize the DC voltage due to inversed regulation direction. The excessive support in this scenario may result in DC voltage collapse and the tripping of GFM PV systems.

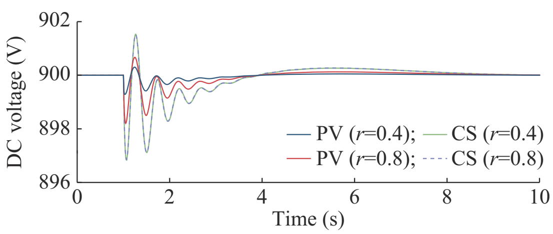

Fig. 10. DC voltage dynamics during GFM transients driven by different primary sources under two power reserve levels.

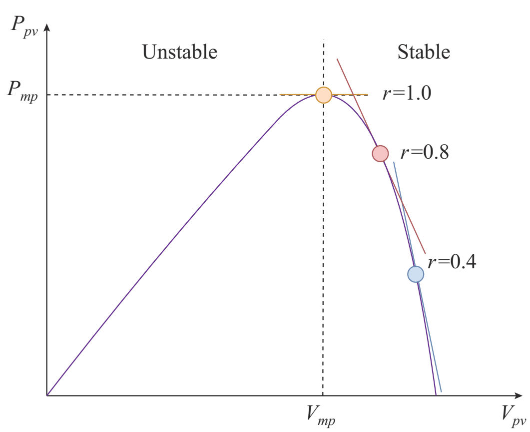

Fig. 11. Deloading nonlinearity on power-voltage curve of PV array.

E. Effect of Boost Converter

Since the output frequency of MSM is coupled with the DC voltage deviation, all the control loops affecting DC voltage dynamics also affect the GFM performance of MSM, which is similar to that of MC. As shown in Fig. 12, when the integral control parameter of the boost converter K_i varies from 1 to 5, the dynamic response of MSM to the load disturbance becomes increasingly pronounced. This is because larger control parameters lead to more robust DC voltage regulation by the boost converter, as well as smaller DC voltage deviation. As a result, the feedforward signal from the DC voltage to the output frequency is diminished, which results in enhanced active support. A comparable enhancement of active support can be achieved by increasing the DC-link capacitor.

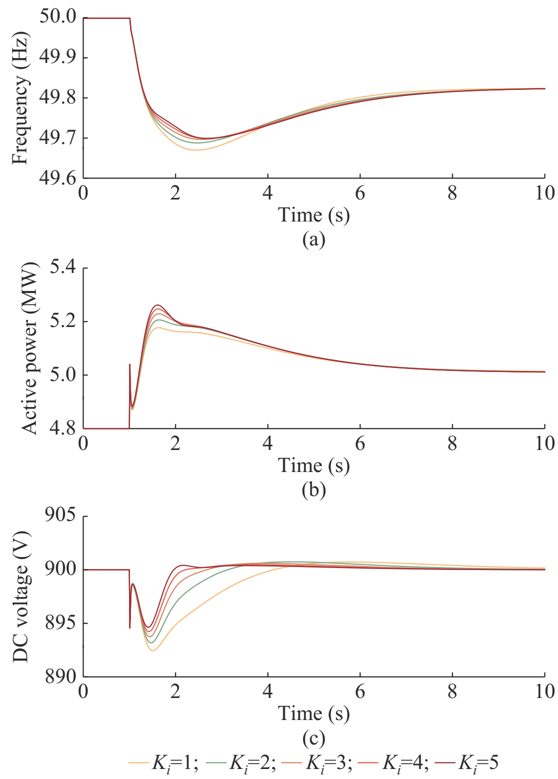

Fig. 12. Active support from PV systems under MSM with variable integral control parameters of boost converter. (a) Frequency at PCC. (b) Total active power of PV systems. (c) DC voltage of single PV system.

F. Hardware Experiment

The proposed method is also tested in a single-stage PV system at the State Key Laboratory of Power Systems, Tsinghua University, Beijing, China. The experimental roof-top PV system is shown in Fig. 13. The inverter is rated 40 kVA, which enables the 15 kW roof-top PV array be connected to the 380 V side of the step-up transformer. Due to the fact that the field test is conducted in December, with a portion of the PV array undergoing maintenance, the maximum PV output power is 3.5 kW in a sunny winter morning. Control parameters of the GFM PV system is presented as follows: the matching factor $k_\theta = 0.1$, the active droop ratio $D_p = 1$ p.u., and the reactive droop ratio $D_q = 30$ p.u..

As Fig. 14 shows, the initial operation point of PV array is deloaded to provide a reserve of power for active support. Since the PV system is integrated with the utility grid, the frequency disturbance is injected by step changing the frequency reference, which is equivalent to the frequency deviation event as shown in (21). The frequency reference undergoes a step-up change at $t=3.2$ s to emulate the low-frequency event, and a step-down change at $t=8.9$ s to emulate the over-frequency event. The recorded active power of the inverter shows a rapid and stable response to the disturbances. A similar test is conducted with the inverter control algorithm replaced with the matching factor set to be zero, which deactivates the DC voltage enhancement from the GFM inverter. As Fig. 15 shows, the active power is aggressively regulated, resulting in the DC voltage exceeding the maximum power point and entering the unstable region. The PV system is finally tripped off by the overcurrent protection of insulated-gate bipolar transistor (IGBT), but not by the DC voltage collapse due to the virtual impedance control. However, the tripping procedure is initiated by the unstable DC voltage dynamics. On the contrary, the enhanced DC voltage dynamics in MSM ensure that the operation point of the PV array remains within the power reserve region, thereby providing stable active support.

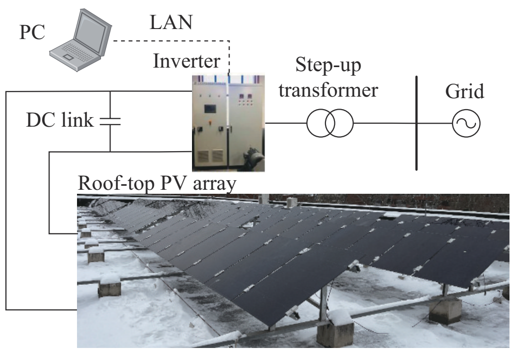

Fig. 13. Experimental roof-top PV system.

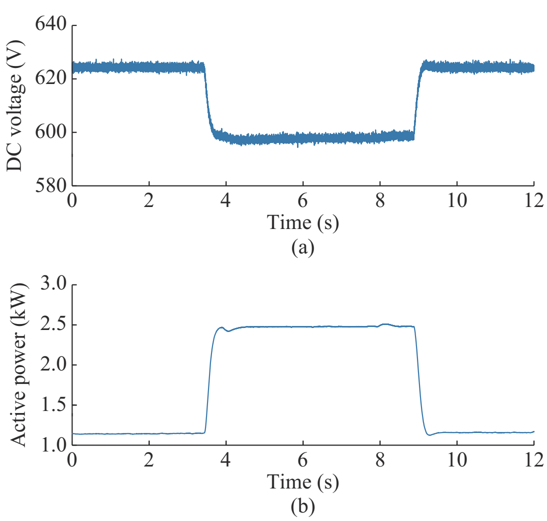

Fig. 14. Active support from GFM PV system with enhanced DC voltage dynamics. (a) DC-link voltage. (b) Active power of inverter.

V. Conclusion

In this paper, we present a comprehensive evaluation of the current GFM methods in terms of their active support performance when embedded on a PV platform. With the primary source modeled in detail, the interactions between the AC-side GFM methods and the DC-side primary dynamics are revealed.

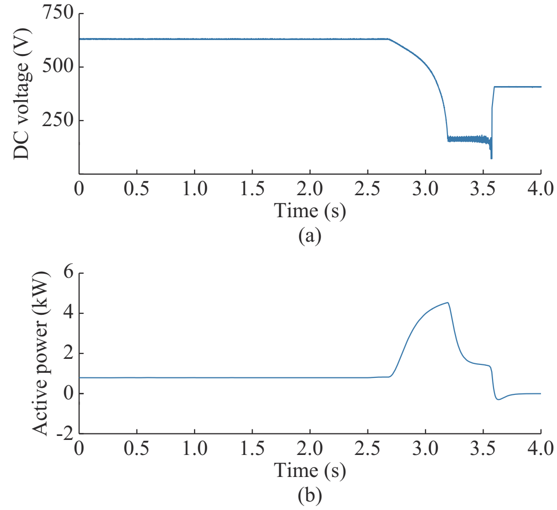

Fig. 15. Active support from GFM PV system without enhanced DC voltage dynamics. (a) DC-link voltage. (b) Active power of inverter.

The AC GFM methods such as droop control, VSM, and dVOC are agnostic to the DC voltage deviation, which may induce the DC voltage collapse in insufficient primary power scenarios. The potential tripping of PV system is a significant risk to the operation of the local network. MC takes into account the DC voltage regulation through structural matching scheme. However, the nonlinearity of PV system results in an undesirable active support characteristic of MC.

To address these issues, we propose the MSM control method to provide the stable and dispatchable active support from distributed PV systems through joint feedbacks of the active power and the DC voltage. The DC voltage regulation is enhanced to prevent the inner state from instability. The steady-state droop response accurately tracks the dispatched value through the AC feedback. This method exploits the benefits of SG emulation-based GFM strategies and the essence of MC, thereby establishing an optimal foundation for the coordination of large-scale distributed PV systems to provide collective active support.

References

[1] International Renewable Energy Agency. (2022, Apr.). IRENA renewable capacity statistics 2022. [Online]. Available: https://www.irena.org/publications/2022/Apr/Renewable-Capacity-Statistics-2022

[2] F. Dörfler and D. Groß, "Control of low-inertia power systems," *Annual Review of Control, Robotics, and Autonomous Systems*, vol. 6, pp. 415-445, May 2023.

[3] M. G. Dozein, B. C. Pal, and P. Mancarella, "Dynamics of inverter-based resources in weak distribution grids," *IEEE Transactions on Power Systems*, vol. 37, no. 5, pp. 3682-3692, Sept. 2022.

[4] Joint NERC and WECC Staff. (2019, Jan.). Fault Induced Solar Photovoltaic Resource Interruption Disturbances Report: Southern California Events: Apr. 20, 2018 and May 11, 2018. [Online]. Available: https://www. nerc. com/pa/rrm/ea/Pages/April-May-2018-Fault-Induced-Solar-PV-Resource-Interruption-Disturbances-Report.aspx

[5] A. Cabrera-Tobar, E. Bullich-Massagué, M. Aragüés-Peñalba *et al.*, "Review of advanced grid requirements for the integration of large-scale photovoltaic power plants in the transmission system," *Renewable and Sustainable Energy Reviews*, vol. 62, pp. 971-987, Sept. 2016.

[6] H. Xin, Y. Liu, Z. Wang *et al.*, "A new frequency regulation strategy for photovoltaic systems without energy storage," *IEEE Transactions on Sustainable Energy*, vol. 4, no. 4, pp. 985-993, Oct. 2013.

[7] C. A. Hill, M. C. Such, D. Chen *et al.*, "Battery energy storage for en-

abling integration of distributed solar power generation," *IEEE Transactions on Smart Grid*, vol. 3, no. 2, pp. 850-857, Jun. 2012.

[8] H. Liu, P. C. Loh, X. Wang *et al*., "Droop control with improved disturbance adaption for a PV system with two power conversion stages," *IEEE Transactions on Industrial Electronics*, vol. 63, no. 10, pp. 6073-6085, Oct. 2016.

[9] D. Wu, F. Tang, T. Dragicevic *et al*., "Coordinated control based on bus-signaling and virtual inertia for islanded DC microgrids," *IEEE Transactions on Smart Grid*, vol. 6, no. 6, pp. 2627-2638, Nov. 2015.

[10] P. Christensen, G. Andersen, M. Seidel *et al*. (2020, Jan.). High penetration of power electronic interfaced power sources and the potential contribution of grid forming converters. [Online]. Available: https://eepublicdownloads. blob. core. windows. net/public-cdn-container/clean-documents/Publications/SOC/High_Penetration_of_Power_Electronic_Interfaced_Power_Sources_and_the_Potential_Contribution_of_Grid_Forming_Converters.pdf

[11] J. Zhou, H. Ding, S. Fan *et al*., "Impact of short-circuit ratio and phase-locked-loop parameters on the small-signal behavior of a VSC-HVDC converter," *IEEE Transactions on Power Delivery*, vol. 29, no. 5, pp. 2287-2296, Oct. 2014.

[12] R. Pan, G. Tang, S. Liu *et al*., "Impedance analysis of grid forming control based modular multilevel converters," *Journal of Modern Power Systems and Clean Energy*, vol. 11, no. 3, pp. 967-979, May 2023.

[13] L. Huang, H. Xin, Z. Wang *et al*., "A virtual synchronous control for voltage-source converters utilizing dynamics of DC-link capacitor to realize self-synchronization," *IEEE Journal of Emerging and Selected Topics in Power Electronics*, vol. 5, no. 4, pp. 1565-1577, Dec. 2017.

[14] D. Pan, X. Wang, F. Liu *et al*., "Transient stability of voltage-source converters with grid-forming control: a design-oriented study," *IEEE Journal of Emerging and Selected Topics in Power Electronics*, vol. 8, no. 2, pp. 1019-1033, Jun. 2020.

[15] B. Pawar, E. Batzelis, S. Chakrabarti *et al*., "Grid-forming control for solar PV systems with power reserves," *IEEE Transactions on Sustainable Energy*, vol. 12, no. 4, pp. 1947-1959, Oct. 2021.

[16] H. Deng, J. Fang, Y. Qi *et al*., "A generic voltage control for grid-forming converters with improved power loop dynamics," *IEEE Transactions on Industrial Electronics*, vol. 70, no. 4, pp. 3933-3943, Apr. 2023.

[17] A. Alassi, K. Ahmed, A. Egea-Alvarez *et al*., "Modified grid-forming converter control for black-start and grid-synchronization applications," in *Proceedings of 2021 56th International Universities Power Engineering Conference*, Middlesbrough, UK, Sept. 2021, pp. 1-5.

[18] Y. Chen, R. Hesse, D. Turschner *et al*., "Investigation of the virtual synchronous machine in the island mode," in *Proceedings of 2012 3rd IEEE PES Innovative Smart Grid Technologies Europe*, Berlin, Germany, Feb. 2012, pp. 1-6.

[19] M. C. Chandorkar, D. M. Divan, and R. Adapa, "Control of parallel connected inverters in standalone AC supply systems," *IEEE Transactions on Industry Applications*, vol. 29, no. 1, pp. 136-143, Aug. 1993.

[20] J. Driesen and K. Visscher, "Virtual synchronous generators," in *Proceedings of 2008 IEEE PES General Meeting – Conversion and Delivery of Electrical Energy in the 21st Century*, Pittsburgh, USA, Jul. 2008, pp. 1-3.

[21] C. Arghir, T. Jouini, and F. Dörfler, "Grid-forming control for power converters based on matching of synchronous machines," *Automatica*, vol. 95, pp. 273-282, Mar. 2018.

[22] B. B. Johnson, S. V. Dhople, A. O. Hamadeh *et al*., "Synchronization of parallel single-phase inverters with virtual oscillator control," *IEEE Transactions on Power Electronics*, vol. 29, no. 11, pp. 6124-6138, Nov. 2014.

[23] M. Colombino, D. Gros, and F. Dorfler, "Global phase and voltage synchronization for power inverters: a decentralized consensus-inspired approach," in *Proceedings of 2017 IEEE 56th Annual Conference on Decision and Control*, Melbourne, Australia, Dec. 2017, pp. 5690-5695.

[24] M. Colombino, D. Groz, J. S. Brouillon *et al*., "Global phase and magnitude synchronization of coupled oscillators with application to the control of grid-forming power inverters," *IEEE Transactions on Automatic Control*, vol. 64, no. 11, pp. 4496-4511, Nov. 2019.

[25] H. Shi, Z. Fang, H. Yi *et al*., "A novel real-time voltage and frequency compensation strategy for photovoltaic-based microgrid," *IEEE Transactions on Industrial Electronics*, vol. 62, no. 6, pp. 3545-3556, Jun. 2015.

[26] Z. Zhao, P. Yang, Y. Wang *et al*., "Dynamic characteristics analysis and stabilization of PV-based multiple microgrid clusters," *IEEE Transactions on Smart Grid*, vol. 10, no. 1, pp. 805-818, Jan. 2019.

[27] T. L. Vandoorn, B. Meersman, D. Kooning *et al*., "Transition from islanded to grid-connected mode of microgrids with voltage-based droop control," *IEEE Transactions on Power Systems*, vol. 28, no. 3, pp. 2545-2553, Aug. 2013.

[28] M. Chen, D. Zhou, A. Tayyebi *et al*., "Generalized multivariable grid-forming control design for power converters," *IEEE Transactions on Smart Grid*, vol. 13, no. 4, pp. 2873-2885, Jul. 2022.

[29] D. Gros, E. Sanchez-Sanchez, E. Prieto-Araujo *et al*., "Dual-port grid-forming control of MMCs and its applications to grids of grids," *IEEE Transactions on Power Delivery*, vol. 37, no. 6, pp. 4721-4735, Dec. 2022.

[30] A. Tayyebi, D. Gross, A. Anta *et al*., "Frequency stability of synchronous machines and grid-forming power converters," *IEEE Journal of Emerging and Selected Topics in Power Electronics*, vol. 8, no. 2, pp. 1004-1018, Jun. 2020.

[31] Z. Chen, R. H. Lasseter, and T. M. Jahns, "Active power reserve control for grid-forming PV sources in microgrids using model-based maximum power point estimation," in *Proceedings of 2019 IEEE Energy Conversion Congress and Exposition*, Baltimore, USA, Nov. 2019, pp. 41-48.

[32] E. Shoubaki, S. Essakiappan, M. Manjrekar *et al*., "Synthetic inertia for BESS integrated on the DC-link of grid-tied PV inverters," in *Proceedings of 2017 IEEE 8th International Symposium on Power Electronics for Distributed Generation Systems*, Florianopolis, Brazil, Jul. 2017, pp. 1-5.

[33] S. Yazdani, M. Ferdowsi, M. Davari *et al*., "Advanced current-limiting and power-sharing control in a PV-based grid-forming inverter under unbalanced grid conditions," *IEEE Journal of Emerging and Selected Topics in Power Electronics*, vol. 8, no. 2, pp. 1084-1096, Jun. 2020.

[34] P. Li, W. Gu, L. Wang *et al*., "Dynamic equivalent modeling of two-staged photovoltaic power station clusters based on dynamic affinity propagation clustering algorithm," *International Journal of Electrical Power & Energy Systems*, vol. 95, pp. 463-475, Feb. 2018.

[35] E. I. Batzelis, G. Anagnostou, I. R. Cole *et al*., "A state-space dynamic model for photovoltaic systems with full ancillary services support," *IEEE Transactions on Sustainable Energy*, vol. 10, no. 3, pp. 1399-1409, Jul. 2019.

[36] H. Yuan, X. Yuan, and J. Hu, "Modeling of grid-connected VSCs for power system small-signal stability analysis in DC-link voltage control timescale," *IEEE Transactions on Power Systems*, vol. 32, no. 5, pp. 3981-3991, Sept. 2017.

[37] B. Barac, M. Krpan, T. Capuder *et al*., "Modeling and initialization of a virtual synchronous machine for power system fundamental frequency simulations," *IEEE Access*, vol. 9, pp. 160116-160134, Nov. 2021.

[38] S. Ali Khajehoddin, M. Karimi-Ghartemani, and M. Ebrahimi, "Grid-supporting inverters with improved dynamics," *IEEE Transactions on Industrial Electronics*, vol. 66, no. 5, pp. 3655-3667, May 2019.

[39] G. S. Seo, M. Colombino, I. Subotic *et al*., "Dispatchable virtual oscillator control for decentralized inverter-dominated power systems: analysis and experiments," in *Proceedings of 2019 IEEE Applied Power Electronics Conference and Exposition*, Anaheim, USA, Mar. 2019, pp. 561-566.

[40] K. Strunz, E. Abbasi, and R. Fletcher, "Benchmark systems for network integration of renewable and distributed energy resources – CIGRE task force C6.04.02," CIGRE, Paris, France, Tech. Rep. 575, Apr. 2014

[41] V. Purba, B. B. Johnson, S. Jafarpour *et al*., "Dynamic aggregation of grid-tied three-phase inverters," *IEEE Transactions on Power Systems*, vol. 35, no. 2, pp. 1520-1530, Mar. 2020.

Zizhen Guo received the B.S. degree from the Electrical Engineering Department, Tsinghua University, Beijing, China, in 2020. He is currently pursuing the Ph.D. degree in electrical engineering at Tsinghua University. His research interests include optimization and control in power system with integration of renewable generation.

Wenchuan Wu received the B.S., M.S., and Ph.D. degrees from the Electrical Engineering Department, Tsinghua University, Beijing, China. He is currently a Professor with Tsinghua University. He was a recipient of the National Science Fund of China Distinguished Young Scholar Award in 2017. His research interests include energy management system, active distribution system operation and control, machine learning and its application in energy system.